UNIVERSITY OF CALIFORNIA SAN DIEGO

Mitochondrial membrane-coated nanomaterials for targeted drug detoxification and detection

A Thesis submitted in partial satisfaction of the requirements for the degree Master of Science

in

Bioengineering

by

Anvita E Komarla

Committee in charge:

Professor Liangfang Zhang, Chair
Professor Ratneshwar Lal, Co-Chair
Professor Ester Jihae Kwon

2021

The thesis of Anvita E Komarla is approved, and it is acceptable in quality and form for publication on microfilm and electronically.

University of California San Diego

2021

TABLE OF CONTENTS

LIST OF FIGURES

ACKNOWLEDGMENTS

This thesis is material as it appears in "Nanomaterial biointerfacing via mitochondrial membrane coating for targeted detoxification and molecular detection", Nano Letters 2021, Gong, Hua; Zhang, Qiangzhe; Komarla, Anvita; Wang, Shuyan; Duan, Yaou; Zhou, Zhidong; Chen, Fang; Fang, Ronnie; Xu, Sheng; Gao, Weiwei; Zhang, Liangfang. The thesis author was a co-author of this paper.

I would like to thank all the co-authors of this paper for their contributions. Hua Gong mentored me throughout my time in the Zhang lab and taught me the techniques used in this paper. Dr. Weiwei Gao supervised the project and provided advice on how to successfully execute the project plan. Qiangzhe Zhang was a great resource during and after the project and contributed significantly to bringing the paper to its final published form.

A huge thank you to all my friends and family that have supported me unconditionally throughout the two years of the program, I would not be here without all of you.

ABSTRACT OF THE THESIS

Mitochondrial membrane-coated nanomaterials for targeted drug detoxification and detection

by

Anvita E Komarla

Master of Science in Bioengineering

University of California San Diego, 2021

Professor Liangfang Zhang, Chair
Professor Ratnesh Lal, Co-Chair

Cell membranes have been widely used to create biomimetic nanoparticles for targeted drug delivery and detoxification. However, intracellular organelle membranes have not been used for biomimetic nanoparticle coating thus far. In this study, outer mitochondrial membranes (OMM) were used to coat PLGA cores to create OMM-coated nanoparticles (OMM-NPs). The B-cell lymphoma-2 (Bcl-2) receptors specific to the OMM enabled targeted detoxification of ABT-263, an anti-cancer Bcl-2 inhibitor. The OMM-NPs successfully decreased cell death *in vitro* and decreased ABT-263 induced-thrombocytopenia *in vivo*. OMM membranes

were also used to coat the surface of Field Effect Transistors (FETs) to make OMM-FETs. These devices were successfully able to distinguish between different concentrations of compounds with Bcl-2 affinity. This study demonstrates that organelle membranes can help extend the functionality of nanomaterials and their unique surface receptors make them useful in targeted drug detoxification and detection.

1. Introduction

Nanomaterials have unique properties such as small size, high surface area to mass ratio, and high reactivity.[1] They are also highly tunable and their circulation time in the blood, immunogenicity, and drug release profiles can be modified easily.[1] The field of nanomedicine involves harnessing the advantages of nanomaterials to use them in disease detection, treatment, and prevention.[2]

Although nanomaterials are a powerful tool, introducing them into a physiological setting can be challenging.[3] Since the human body is designed to recognize and defend against foreign objects, synthetically-made nanomaterials can trigger the immune system and result in rapid clearance.[4] Surface modifications such as PEGylation on the nanomaterial surface have been used to reduce cellular uptake and increase half-life. However, the anti-PEG immune response to some PEGylated nanomaterials has inspired alternative approaches to nanomaterial functionalization.[5] Another form of surface modification involves coating nanomaterials with surface proteins, such as CD47 found on Red Blood Cells (RBCs), to create biomimetic nanoparticles capable of evading macrophage clearance. Although successful, replicating a natural cell's entire protein corona has proven challenging. To overcome this, cell membranes themselves have been used to coat nanoparticles, thus creating cell membrane-coated nanoparticles. The cell membrane camouflages the nanoparticles by retaining the natural surface characteristics of the cells from which the membrane was derived. This strategy avoids the need to artificially recreate the cell membrane surface while allowing evasion of the host immune system.

Previous studies have shown that cell-membrane coated nanoparticles can be used as "nanosponges".[6,7] Nanosponges can bind to toxic molecules and sequester them to prevent binding to target cells. Cell membrane-coated nanomaterials have also been able to detect the binding of toxic molecules to their surface, allowing for quantitative detection.[8] Given these advantages, membranes from RBCs, cancer cells, epithelial cells, platelets, and macrophages have been used to coat nanomaterials for drug detoxification, vaccination, drug delivery, and toxin detection.[6–11] Until now, cell-membrane coating technology has primarily used plasma membranes from cells, and organelle membranes have not been utilized. Intracellular organelle membranes contain proteins that give them organelle-specific functions. This research involved the creation of the first organelle membrane-coated nanomaterials.

2. Results & Discussion

2.1. Fabrication and characterization of OMM-NPs

OMM-coated nanoparticles (OMM-NPs) were prepared using three main steps. First, the OMM was isolated from mouse mitochondria. Livers were collected from mice and the mitochondria were isolated using sucrose density ultracentrifugation.[12] The OMM and IMM were separated from each other using osmotic shock and the OMM was isolated using ultracentrifugation.[13] The purity of the OMM was confirmed by analyzing cytochrome c, DNA, and Bcl-2 content in the purified sample.

Second, PLGA nanoparticle cores were prepared using a pre-established nanoprecipitation method.[14]

Third, the OMM and PLGA cores were mixed at a 1:1 protein weight ratio and sonicated to form OMM-NPs.

2.1.2. Size and zeta potential measurements

To verify that the PLGA cores had been successfully coated with the OMM, the size of the particles was measured by Dynamic Light Scattering (DLS) and zeta potential using the Zetasizer instrument. The size and zeta potential of nanoparticles are important characteristics since they influence cellular uptake.[15] DLS can be used to determine the size of nanoparticles by measuring the extent of incident light scattering due to Brownian motion.[16] The PLGA cores were 103 ± 9.4 nm in size before coating (Figure 1). After coating, the OMM-NPs (i.e., coated PLGA cores) were 128 ± 9.4 nm, which gave an average size difference of 9 ± 1.6 nm after coating (Figure 1). This value aligns with the ~7 nm OMM thickness that has been reported in previous studies where mitochondrial membrane thickness was measured using electron tomography.[17] The surface zeta potential of the PLGA cores was -42.2 ± 1.3 mV and that of the OMM-NPs was -25.0 ± 3.4 mV (Figure 1). The zeta potential of a particle indicates its surface charge which is an important parameter in determining nanoparticle stability in solutions.[18] The likelihood of particles to aggregate, and therefore induce toxicity, largely depends on zeta potential.

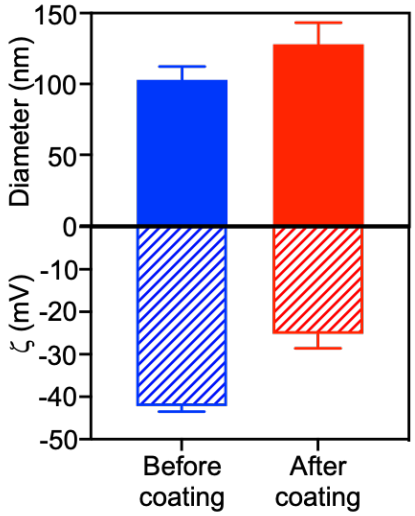

Figure 1. Hydrodynamic size (diameter, nm) and zeta potential (ζ, mV) measurements of particles before (blue) and after (red) coating using Dynamic Light Scattering (n=3, mean + standard deviation).

2.1.3. Visualization of OMM-NP structure

The structure of OMM-NPs were visualized by Transmission Electron Microscopy (TEM) (Figure 2).

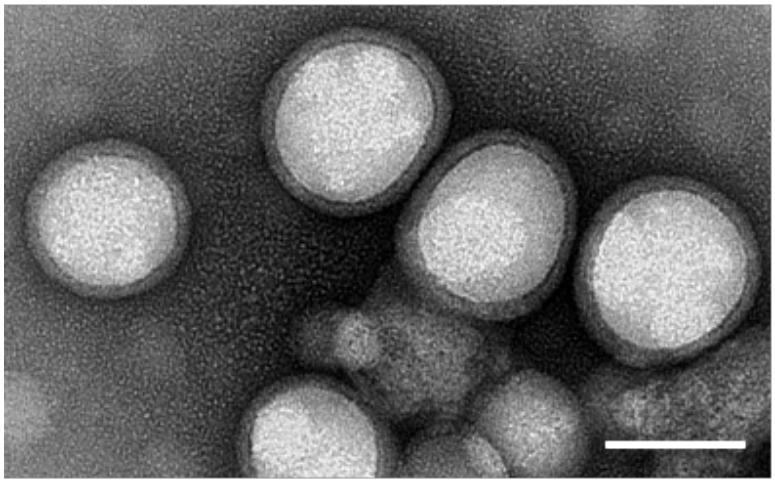

Figure 2. Transmission Electron Microscope image of OMM-NPs negatively stained using uranyl acetate. Scale bar represents 100 nm.

2.1.4. Characterizing surface proteins

To confirm that the OMM-NPs retained surface markers expressed by the OMM, sodium dodecyl sulfate-polyacrylamide gel electrophoresis (SDS-PAGE) and antibody staining were used. The OMM-NPs and the OMM lysate were loaded onto an SDS-PAGE gel and the resulting patterns were compared. As shown by the gel in Figure 3, the OMM-NP and OMM lysate protein profiles matched closely. This indicates that the surface markers present on the OMM were retained on the membrane after the coating process.

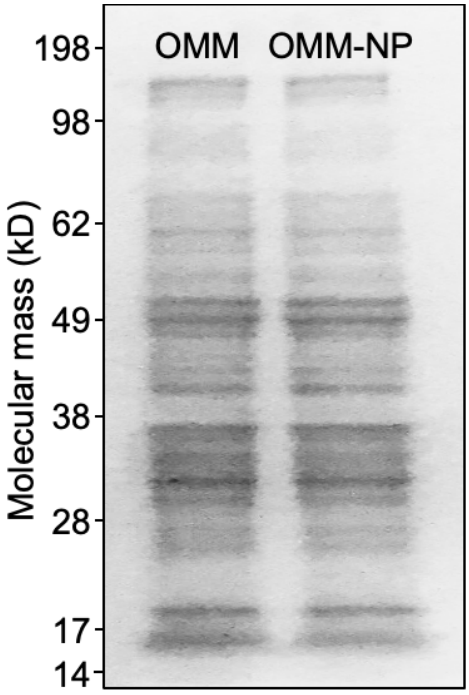

Figure 3. SDS-PAGE comparing OMM and OMM-NPs. Equal concentrations of both samples were used. Staining was done using Coomassie Blue.

Bcl-2 proteins, which are involved in the regulation of cell apoptosis, are localized to the OMM and the Endoplasmic Reticulum (ER).[19] The Bcl-2 content of the Mitochondria (MT), OMM, and OMM-NPs were analyzed by Western blot as shown in Figure 4. MT showed some

Bcl-2 signal but it was significantly enriched in the OMM and OMM-NPs indicating that Bcl-2 was retained on the OMM-NP surface.

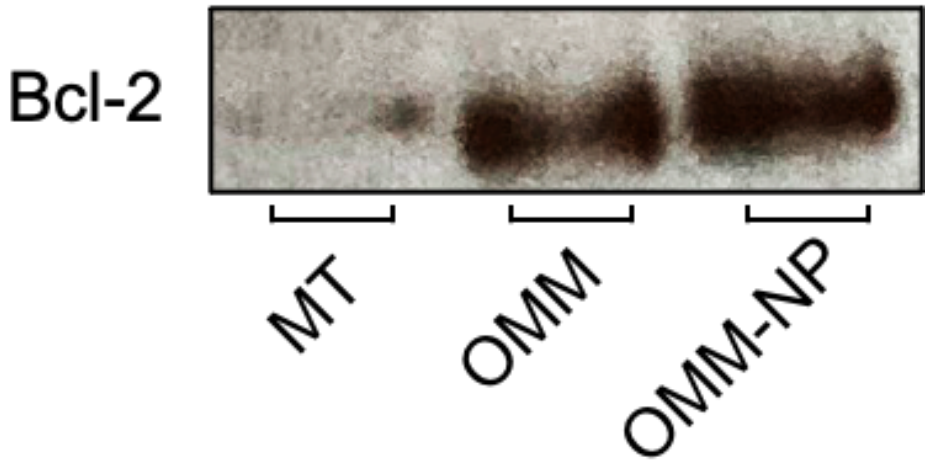

Figure 4. Comparing Bcl-2 content in whole mitochondria (MT), OMM, and OMM-NP by Western Blot.

2.1.4. Membrane sidedness verification

Since the phospholipid bilayer of cells or organelles contains two sides, a cytoplasm-facing side, and an extracellular environment-facing side, it was necessary to determine which side of the OMM had bound to the nanoparticle surface and therefore which side was outward-facing. To replicate the functionality of the OMM, the OMM-NP would have to retain the same orientation of the natural membrane such that surface receptors of the OMM are also surface receptors in the OMM-NP. To determine membrane orientation, OMM and OMM-NPs were incubated with anti-Bcl-2 antibodies. The free antibodies were removed, and the fluorescence intensity of the samples was measured as shown in Figure 5. Both samples showed similar fluorescence intensity indicating that the surface expression of Bcl-2 was comparable across the two. If the membrane had been coated in the "wrong-side-out" configuration, the extent of antibody staining would likely be lower than the "right-side-out" case. The comparable

fluorescence intensity of the OMM and the OMM-NP indicates that the OMM-NP had been coated in a right-side-out configuration.

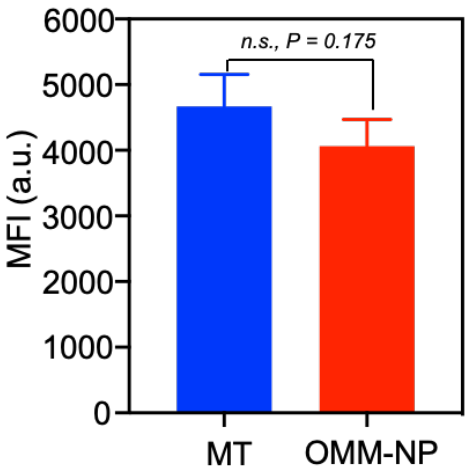

Figure 5. Comparing fluorescence intensity of whole MT and OMM-NP after staining with Alexa Fluor 647 labeled anti-Bcl-2 antibodies.

2.1.5. Nanoparticle stability

To determine the stability of the nanoparticle coating, the OMM-NP size was monitored in water, 1X Phosphate Buffered Saline (PBS), and 50% serum over 48 hours (Figure 6). PBS was used to simulate biological environments since the osmolarity and ion concentrations are comparable to those in the human body.[20] When nanoparticles are introduced *in vivo* they encounter serum proteins present in the blood.[21] The extent of nanoparticle aggregation and therefore their macrophage uptake and cellular toxicity are influenced by protein-nanomaterial interactions. Thus, the stability of the nanoparticles in 50% serum was observed to ensure that the OMM-NPs did not aggregate when they encountered serum proteins.

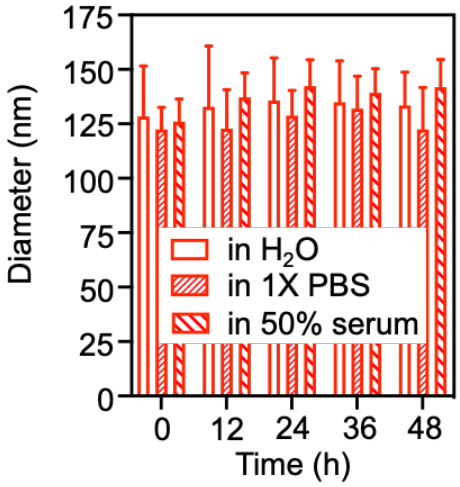

Figure 6. Stability of OMM-NPs in water, 1X PBS, and 50% serum using hydrodynamic size as measured using Dynamic Light Scattering over 48 hours (n=3, mean + standard deviation).

2.2. *In vitro* detoxification of ABT-263, a Bcl-2 inhibitor

Once the OMM-NPs were fabricated and verified to have optimal stability, mitochondria surface marker retention, and appropriate membrane sidedness they were tested in an *in vitro* model of drug detoxification. We used ABT-263, a Bcl-2 inhibitor that is used as an anti-cancer therapy due to its effect on cell apoptotic pathways, as a model drug.[22]

Apoptosis, also known as programmed cell death, is an essential cellular process that helps get rid of old and damaged cells. This helps maintain tissue homeostasis, ensures proper development of tissues, and maintains immune systems.[23] Dysregulated apoptotic pathways are often involved in cancer, autoimmune disorders, and neurodegenerative diseases. In cancer specifically, damaged apoptotic pathways allow tumorigenic cells to be more resistant to otherwise death-inducing conditions such as hypoxia, genetic damage, and insufficient matrix attachment.[22]

The Bcl-2 family of proteins contains both pro-apoptotic and anti-apoptotic proteins that help regulate cell apoptosis. Bcl-2 and Bcl-xL are two anti-apoptotic proteins that are often overexpressed in tumor cells to help enhance their survival.[24] Dysregulation of Bcl-2 pathways is involved in B-cell lymphoma and acute lymphoid leukemia.[25] ABT-263, commercially known as Navitoclax, is a Bcl-2/Bcl-xL inhibitor that has been shown to effectively target small cell lung cancer and T and B cell lymphomas. Since Bcl-2 proteins are localized to the OMM, we used ABT-263 as a model drug to determine if the OMM-NPs could successfully bind to and sequester the drug and prevent them from binding to other cells in the environment.[19]

2.2.1. Quantification of ABT-263 binding

To determine if the ABT-263 binding capacity of the OMM-NPs was concentration-dependent, different amounts of OMM-NPs were added to three different fixed amounts of ABT-263. The drug and OMM-NPs were incubated, and the remaining drug was quantified using high-performance liquid chromatography (HPLC). The amount of drug sequestered by the OMM-NPs was determined by subtracting the leftover drug detected by HPLC from the input drug. A sigmoid pattern was observed when the concentration of nanoparticles on a log scale was plotted against the amount of ABT-263 absorbed (Figure 7).

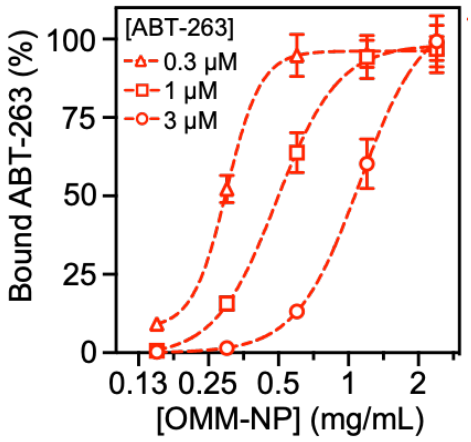

Figure 7. Three fixed concentrations of ABT-263, 0.3 μM, 1 μM, 3 μM, were used in the OMM-NP binding study. The OMM-NP concentration was varied from 0.13 to 2 mg/mL.

2.2.2. Cell viability in response to ABT-263 treatment

Once the HPLC quantification studies showed that ABT-263 successfully binds to the OMM-NPs, the OMM-NPs were used in an *in vitro* model of drug detoxification. HL60 cells, derived from an acute myeloid leukemia patient, were used in this study since ABT-263 has traditionally been used to treat lymphomas.[25,26] Varying concentrations of ABT-263 were mixed with HL-60 cells and incubated for 48 hours. After the incubation period, the amount of ATP in each of the wells was assessed by the ATPlite kit. The ATPlite assay (Perkin Elmer) involves luminescence-based detection of ATP using the luciferin-luciferase reaction. The amount of luminescence is directly proportional to the concentration of ATP which can then be related to the rate of proliferation. Necrotic and apoptotic cells show a drastically reduced amount of ATP in their environment. The relationship between cell viability (as quantified by the ATPlite assay) and ABT-263 concentration is shown in Figure 8. From this curve, the EC50, the effective concentration at which 50% of the cells lose viability, of ABT-263 was calculated to be 2 μM. This concentration was used in the neutralization assay.

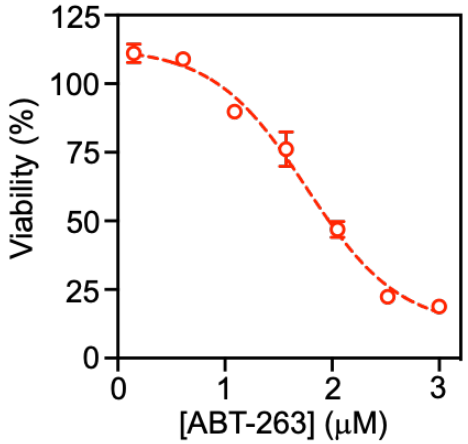

Figure 8. Viability of HL-60 cells in response to treatment with varying concentrations of ABT-263 measured using the ATPlite assay.

2.2.3. *In vitro* ABT-263 neutralization assay

To validate the ability of the OMM-NPs to bind to ABT-263 and prevent it from killing surrounding HL-60 cells, a neutralization study was carried out. Varying concentrations of OMM-NPs ranging from 0.03 - 2 mg/mL were incubated with 2 μM of ABT-263. The mixture was added to HL-60 cells to observe cell death in response to the free ABT-263 drug in the mixture. ABT-263 has been known to induce caspase-3 mediated apoptosis in cells.[27] The Caspase-Glo 3/7 assay (Promega) was used to quantify caspase activity in the cells. This assay involves a substrate that is cleaved and results in a luminescence signal dependent on the caspase-3 or caspase-7 concentration. This luminescence is proportional to the number of apoptotic cells in the well. As shown in Figure 9, the viability of cells increased with increasing concentration of the OMM-NPs. The OMM-NP IC50 and IC100 concentrations, i.e., the amount of OMM-NP required to inhibit 50% and 100% of cell death were 0.65 ± 0.08 mg/ mL and 1.2 ± 0.10 mg/mL, respectively.

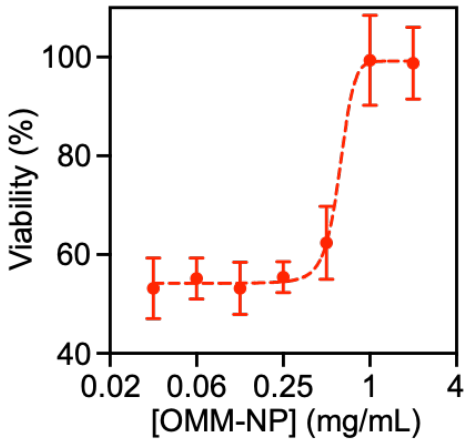

Figure 9. Viability of HL-60 cells in response to co-treatment of 2 µM of ABT-263 with varying concentrations of OMM-NPs measured using the ATPlite assay.

2.3. *In vivo* detoxification of ABT-263

Once the neutralization capability of the OMM-NP formulation was validated *in vitro*, its efficacy was tested *in vivo*. One of the *in vivo* effects of ABT-263 is thrombocytopenia, i.e. an abnormally low platelet count in the blood.[28,29] The extent of *in vivo* detoxification was measured by quantifying platelet counts in response to ABT-236 alone vs. ABT-263 and OMM-NP together. As outlined in Figure 10, mice were treated by oral gavage and either given 1 µmol/kg of ABT-263 alone or 1 µmol/kg of ABT-263 immediately followed by 800 mg/kg of OMM-NPs. Blood was collected from the tail vein of each mouse at 5 min, 6 hours, and 24 hours post drug treatment.

2.3.1. Quantifying platelet and apoptotic cell populations

The blood samples were stained using anti-mouse CD41-Alexa Fluor 647 and Annexin V. CD41 is a platelet-specific marker while Annexin V is commonly used to detect apoptotic cells.[30,31] As shown in Figure 10, the mice treated with ABT-263 alone showed a gradual

decrease in platelet count over time while those treated with ABT-263 and OMM-NPs showed a constant platelet count. Annexin V staining on blood samples from these two groups showed that ABT-263 alone increased apoptotic cell populations over time while mice treated with ABT-263 and OMM-NPs showed a constant apoptotic cell population. These results show that OMM-NPs can successfully reduce ABT-263-induced thrombocytopenia and cell apoptosis *in vivo*.

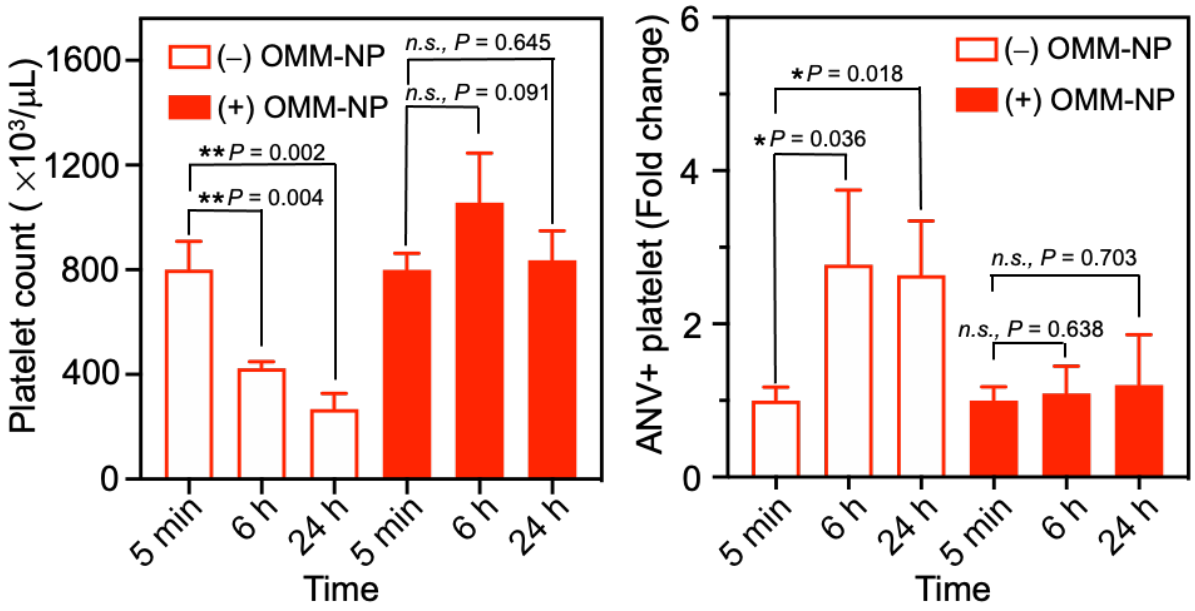

Figure 10. Platelet counts and apoptotic platelet populations after treatment with ABT-263 alone (1 μmol/kg) or ABT-263 (1 μmol/kg) and OMM-NPs (800 mg/kg) based on flow cytometry.

2.4. Preparation and characterization of OMM-FETs

Once the *in vitro* and *in vivo* experiments showed that OMM coated nanoparticles could bind to and sequester mitochondria-targeting drugs, the OMM was used to create a molecular detection platform. Nanomaterials have been used increasingly to improve the sensitivity, cost efficiency, and reproducibility of detection methods for biomolecules such as protein and

nucleic acids.[32] In this study, the detection platform consisted of OMM vesicles fused onto a *p*-type carbon nanotube-based field-effect transistor (FET). FETs have become a popular biodetection method due to their ability to directly sense the interaction of a biomolecule with the FET surface and giving an electrical signal read-out.[33]

2.4.1. Preparing OMM vesicle fused FETs

To prepare OMM-FETs, OMM vesicles were isolated from mouse livers as mentioned earlier. The OMM vesicles were labeled with DiD (1,1′-dioctadecyl-3,3,3′,3′-tetramethylindodicarbocyanine, 4-chlorobenzenesulfonate salt) which is a lipophilic fluorescent dye with an excitation wavelength of 644 nm and emission wavelength of 665 nm. Dye-labeled vesicles were added to the FET surface and allowed to incubate at room temperature to allow vesicle-FET fusion. After the incubation period, the FETs were washed to remove free vesicles. OMM-NPs also underwent a similar procedure to act as a non-fusogenic control. OMM-NPs were labeled with DiD, allowed to incubate on an FET surface, and the FET was washed. Since the OMM had bound to the NP core, it would not be able to fuse to the FET surface. FETs coated with OMM vesicles and OMM-NPs were imaged using fluorescence microscopy. As shown in Figure 11, the FET treated with OMM vesicles (fusogenic) showed strong DiD fluorescence while the one treated with OMM-NPs did not show any fluorescence.

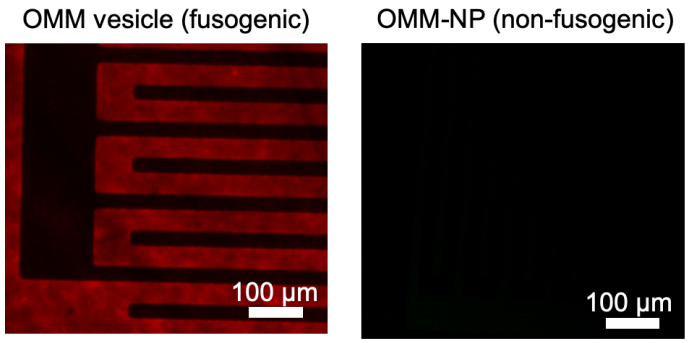

Figure 11. Verification of OMM vesicle fusion to the FET surface using DiD labeled OMM membranes. Imaging was performed using a fluorescence microscope.

The ability of membrane vesicles to fuse onto the FET surface was further validated by using protein encapsulating vesicles. The vesicle membrane was labeled with DiD and had Bovine Serum Albumin (BSA) labeled with Fluorescein in the interior aqueous compartment. When a similar membrane fusion experiment was conducted, FETs only retained the DiD signal from the membrane and did not show any Fluorescein signal (Figure 12). This indicates that the vesicles did not retain their structure after the fusion process and only the membrane was able to fuse with the FET surface.

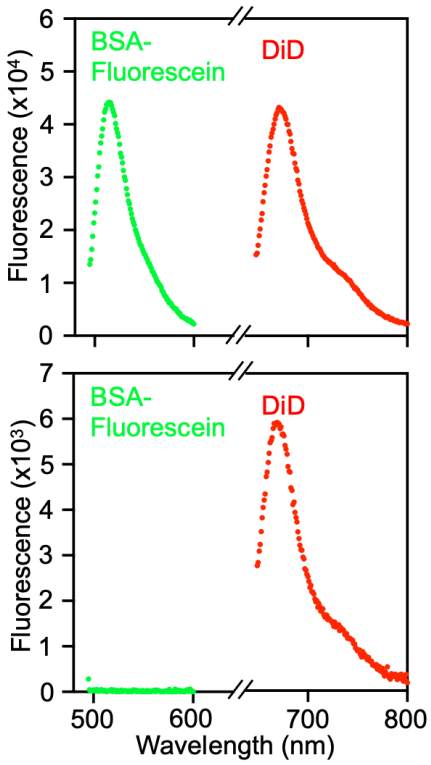

Figure 12. Verification of OMM vesicle fusion to the FET surface using DiD labeled OMM membranes encapsulating FITC-labelled BSA. Analysis was performed using a plate reader.

2.4.2. Characterizing electrical properties of OMM-FETs

The electrical properties of the uncoated FET and OMM-FET were compared to ensure that the semi-conductive properties were retained. When the source-drain voltage was kept fixed, the source-drain current decreased with decreasing gate voltage for both types of FETs indicating that semi-conductive properties were retained (Figure 13).

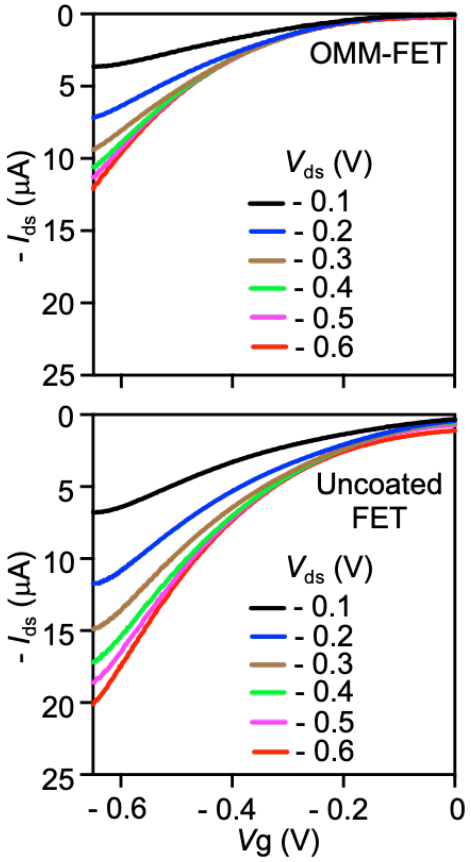

Figure 13. Comparison of electrical properties of coated and uncoated FETs.

2.5. Detection of OMM-binding antibodies and drugs using OMM-FETs

Once the electrical properties had been verified, the ability of the OMM-FET to detect molecular binding on the surface was tested. Anti-Bcl-2 IgG antibodies were used as a test

compound before Bcl-2 targeted drugs. When denatured anti-Bcl-2 antibodies were added in regular intervals to the FET surface there was no change in channel conductance (Figure 14). However, when non-denatured antibodies were added at regular intervals there was a stepwise change in drain-source current. A decrease in channel conductance occurs due to antibody molecules repelling holes in the *p*-type OMM-FETs. We found a linear correlation between antibody concentration and resulting drain-source current. This graph also showed a difference in slope when the denatured and non-denatured antibodies were compared, indicating that the OMM-FET can distinguish between compounds with different Bcl-2 affinity.

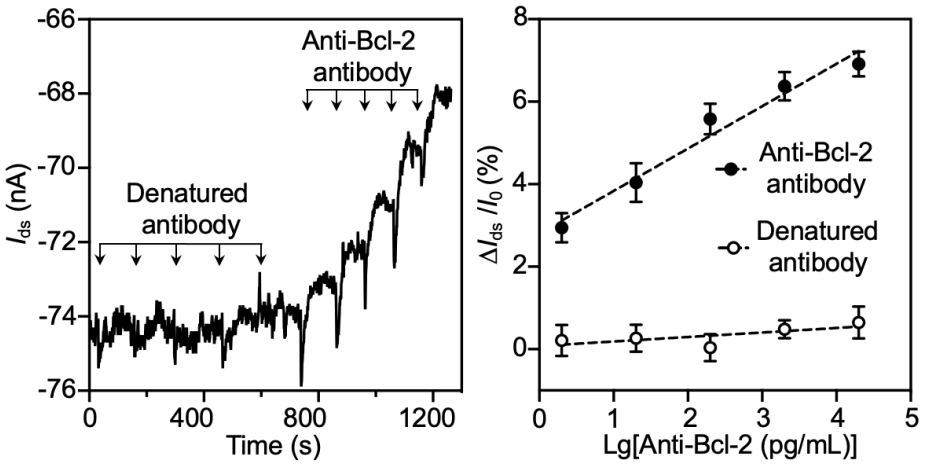

Figure 14. Detection of Anti-Bcl-2 antibodies using an OMM-FET. Left: Graph representing drain-source current vs. time. Right: drain-source current relative to baseline current.

Once the previous study had shown that molecules with Bcl-2 antibodies can bind detectably to the OMM-FET we tested two drugs that target Bcl-2. We tested ABT-263 and HA14-1 which is also a Bcl-2 antagonist but with lower binding affinity. Like the antibody binding study, when both drugs were added to the OMM-FET the drain-source current decreased in a stepwise fashion (Figure 15). There was also a linear relationship between drug concentration and relative change in current (Figure 15). ABT-263 had a steeper slope

compared to the HA14-1, again indicating that the OMM-FET can distinguish between drugs with differing Bcl-2 affinity.

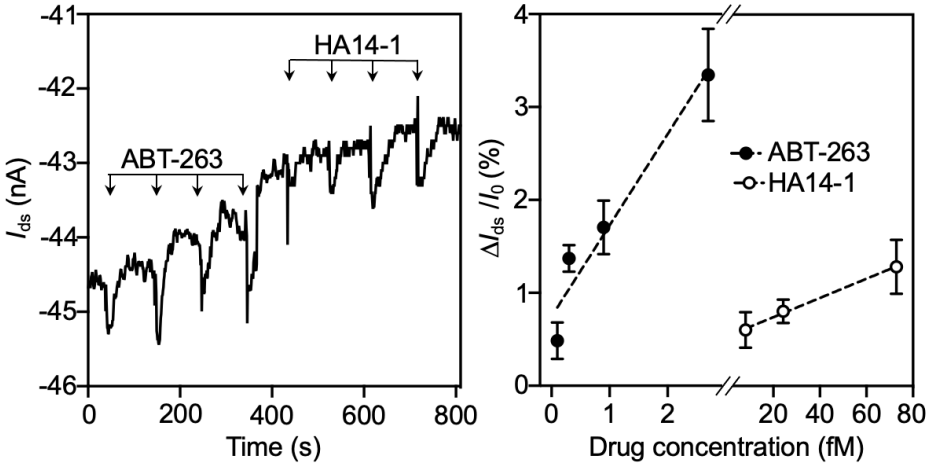

Figure 15. Detection of small molecule inhibitors of Bcl-2 using an OMM-FET. Left: Graph representing drain-source current vs. time. Right: drain-source current relative to baseline current.

3. Conclusion

In summary, we have shown that outer mitochondrial membranes can be used to coat the surfaces of nanoparticles to create OMM-NPs and on field-effect transitions to create OMM-FETs. Our studies showed that OMM-NPs can competitively bind to a Bcl-2 targeting drug and successfully reduce its *in vitro* and *in vivo* toxicity. The OMM-FET can sensitively detect binding events between Bcl-2 targeting molecules and the OMM on the surface. These platforms can be powerful tools in drug detoxification and detection and can be modified to include specialized membranes from other organelles.

4. Materials and methods[34]

4.1. Animal Use

All animal experiments were conducted per the National Institute of Health (NIH) guidelines and approved by the Institutional Animal Care and Use Committee (IACUC) of the University of California, San Diego.

4.2. Collection of mitochondria from mouse livers

Twelve-week-old CD1 mice (male and female, Envigo) were fasted overnight before they were sacrificed. Livers were harvested from each mouse and rinsed with 1X PBS that had been cooled down on ice. The rinsing procedure was repeated thrice to ensure the removal of residual blood. The livers were placed into Petri dishes and minced using a scalpel. Using a transfer pipette, the small pieces of tissue were transferred to a 50 mL conical containing 20 mL of chilled homogenization buffer (210 mM mannitol, 70 mM sucrose, 5 mM Tris-HCl pH 7.5, 1mM EDTA pH 7.5). The tissue in the tube, while on ice, was homogenized for 15 strokes using a Kinematic Polytron PT-2000 homogenizer at power setting 7. The homogenate was spun down at 2000 x *g* for 10 min at 4°C. The supernatant was put aside, and the pellet was homogenized again. The supernatants from both homogenization steps were pooled and spun down again at 7000 x *g* for 10 min at 4°C. The pellet which contained crude mitochondria was further purified using sucrose density ultracentrifugation. 15 mL of 1 M sucrose solution and 15 mL of 1.5 M sucrose solution were added to the tube containing the pellet. The sample was centrifuged at 60,000 x *g* for 20 min at 4°C (Beckman Coulter Optima XPN-80 Ultracentrifuge with an SW32Ti rotor). After centrifugation, the layer between the two sucrose layers which contained the mitochondria was collected. The mitochondria were washed twice using the

homogenization buffer and centrifugation at 7000 x *g* for 10 min at 4℃. The purified mitochondria were stored in homogenization buffer on ice before moving on to the next step. The mitochondria were quantified using the Bicinchoninic acid assay or BCA (Thermo Fisher Scientific).

4.3. Derivation of outer mitochondrial membrane (OMM)

The purified mitochondria from the isolation step were spun down at 7000 x *g* for 10 min at 4℃. The supernatant was discarded, and the pellet was resuspended to a concentration of 5 mg/mL using UltraPure DNase/RNase-Free Distilled Water (Invitrogen). The solution was stirred for 20 minutes on ice. After stirring, an equal volume of 1.4 M sucrose solution was added, and the mixture was stirred on ice for 5 minutes. The mixture, while on ice, was homogenized for 30 strokes using a Kinematic Polytron PT-2000 homogenizer at power setting 7. The homogenized sample was spun at 12,000 x *g* for 10 min at 4℃. The supernatant was collected and spun down at 100,000 x *g* for 30 min at 4℃. The resulting pellet consisted of two different layers, the off-white layer containing the OMM was collected. The OMM was quantified using the BCA assay and stored at -80℃ for future studies. For these studies, 5.3 ± 0.73 mg of OMM was isolated from 100 mg of whole mitochondria (5.3% yield).

4.4. Characterization of outer mitochondrial membrane

To determine the purity of the outer mitochondrial membrane, the cytochrome c content was measured. The absorbance at 415 nm was measured for 1 mg/mL of the whole mitochondria and outer mitochondrial membrane samples.

The DNA content was quantified using the Pico488 dsDNA quantification reagent (Luminprobe) as per the manufacturer's protocol.

Western Blotting was performed using anti-mouse anti-Bcl-2 antibodies (Santa Cruz Biotechnology) and the corresponding horseradish peroxidase (HRP) conjugated Donkey anti-mouse secondary antibodies. The films were developed using ECL western blotting substrate (Thermo Fisher Scientific) on a Mini-Medical/90 developer (ImageWorks).

To quantify the Bcl-2 expression, 100 µL of the whole mitochondria and OMM at 0.1 mg/mL were blocked with Bovine Serum Albumin (BSA, Millipore Sigma) for 30 min at room temperature. After the incubation, the samples were stained with Alexa Fluor 647 labeled anti-Bcl-2 antibodies (1:100, Santa Cruz Biotechnology) for 2 hours at room temperature. After staining, the whole mitochondria were washed thrice using ultracentrifugation at 7,000 x *g* for 10 min to remove excess antibodies. The OMM was washed using Amicon Ultra Centrifugal Units with a 100kDa cutoff (Millipore Sigma). The fluorescence of the samples was measured using a plate reader (BioTek).

4.5. Formulation and characterization of OMM-NPs

The nanoparticles cores made of Poly (lactic-co-glycolic acid) (PLGA, 0.67 dL/g, 50:50 monomer ratio, Absorbable Polymers) were prepared using an established nanoprecipitation method.[5] In a glass vial, 1 mL of 10 mg/mL PLGA in acetone was added dropwise to 4 mL of deionized water. The solution was stirred in a chemical fume hood to allow the acetone to evaporate. The final volume of the solution was adjusted to 4 mL for a 2.5 mg/mL solution of PLGA nanoparticle cores.

To coat the mitochondrial membrane onto the PLGA core surface, the cores and membrane were mixed at a 1:1 weight ratio in a glass vial. The mixture was sonicated for 2 min

using a bath sonicator (Fisher Scientific FS30D). The size of the particles was measured using dynamic light scattering (DLS, ZEN 3600 Zetasizer, Malvern).

OMM-NP morphology was visualized using transmission electron microscopy (TEM). The OMM-NPs were placed onto a 400-mesh copper grid (Electron Microscopy Science). The particles were allowed to incubate on the mesh for 5 minutes, after which the grid was rinsed with 10 drops of DI water. The grid was stained with 1wt% of uranyl acetate (Electron Microscopy Science). The grid was dried and visualized using an FEI 200kV Sphera microscope.

The colloidal stability of the nanoparticles was measured by monitoring the size of the nanoparticles in 1X PBS and DI water at 0, 12, 24, 36, and 48 hour time points. Dynamic Light Scattering was used to measure nanoparticle size at each time point.

Antibodies were used to determine the sidedness of the membrane coating on the nanoparticles. 100 μL of whole mitochondria and OMM-NPs with an equivalent amount of membrane protein were blocked with 4% BSA at room temperature for 30 minutes. Alexa Fluor 647 anti-Bcl-2 antibodies (1:100, Santa Cruz Biotechnology) were added to the samples and incubated at room temperature for 2 hours. After the incubation, the samples were washed by resuspending in PBS and centrifuging three times to remove unbound antibodies. The samples were resuspended in 200 μL of DI water in a 96 well plate and the fluorescent intensity was measured using a plate reader.

4.6. Measuring ABT-263 binding capacity of OMM-NPs

Various concentrations of OMM-NPs (0.15, 0.3, 0.6, 1.2 and 2.4 mg/mL) were mixed with three different concentrations of ABT-263, 0.3, 1, and 3 μM, and incubated at 37°C for 30

minutes. The mixtures were centrifuged at 16,000 x *g* for 10 minutes to create a pellet of nanoparticles and a supernatant containing the unbound drug. The concentration of ABT-263 in the supernatant was measured using high-performance liquid chromatography (HPLC, Agilent Technologies 1220 Infinity II LC). Mobile phase A consisted of 10mM ammonium bicarbonate in water at pH 9.5 and mobile phase B was a mixture of acetonitrile (ACN) and methanol at an 85:15 volume ratio. The mobile phase was kept at 15% A and 85% B with a flow rate of 0.3 mL/minute. ABT-263 was detected at 290 nm. The amount of ABT-263 bound to the OMM-NPs was calculated by subtracting the amount in the supernatant from the input amount. The IC50 and IC100 values were determined using the Sigmoidal dose-response (variable slope) model in GraphPad Prism.

4.7. OMM-NP mediated *in vitro* neutralization of ABT-263

HL-60 cells were purchased from ATCC (American Type Culture Collection) and maintained at 37°C with 5% CO_2. The cells were plated on 96-well tissue culture plates at a seeding density of $1x10^4$ cells/well. ABT-263 was then added to the wells at varying concentrations and incubated for 48 hours. Cell viability was measured using the ATPlite 1step (PerkinElmer) ATP detection assay.

For the caspase detection assay, cells were plated at a density of $5x10^4$ cells/well in 12-well plates. The Caspase-Glo 3/7 assay (Promega) was used to detect caspase activity. To each well, ABT-263 was then added at 3 μM and OMM-NPs were added at 2.4 mg/mL. Untreated cells and cells only treated with ABT-263 were used as controls. After allowing the plate to incubate for 48 hours the supernatant was aspirated and the cells were resuspended in 1X PBS. The Caspase-Glo reagent was added to the cells and the plate was allowed to incubate at room

temperature for 30 minutes. The luminescence of each sample was read using a plate reader. The data was analyzed using the Sigmoidal dose-response (variable slope) model in GraphPad Prism.

4.8. OMM-NP mediated *in vivo* neutralization of ABT-263

Six-week-old female C57BL/6 mice (Charles River Laboratory) were used to assess the *in vivo* efficacy of OMM-NPs to neutralize ABT-263. ABT-263 and OMM-NPs were mixed at a final concentration of 25 μM and 20 mg/mL, respectively, and 800 μl of the mixture was immediately administered to the mice by oral gavage. Mice administered with ABT-263 alone were used as controls. At 5 minutes, 6 hours, and 24 hours post-administration, blood was collected from each mouse by tail vein bleed. The blood samples were diluted at a 1:1000 volume ratio in Annexin V binding buffer (Biolegend). 100 μL of the diluted blood was mixed with FITC labeled Annexin V (1:100, Thermo Fisher Scientific) and Alexa Fluor 647 labeled anti-mouse CD41 (1:100, Biolegend). The cells were incubated at room temperature for 15 minutes and washed twice by centrifugation at 500 x *g* for 3 minutes. The samples were analyzed by flow cytometry using the BD FACS Canto II. The platelet and apoptotic cell population percentages were calculated using FlowJo software.

4.9. Fabrication and characterization of OMM-FETs

A *p*-type single-walled carbon nanotube FET was prepared as described previously.[8] To coat the FET, the isolated OMM were first labeled with DiD dye (Thermo Fisher Scientific, excitation/emission = 647/667 nm) at a 1:1,000 DiD: protein weight ratio. The labeled OMM was resuspended in 1X PBS at 1 mg/ml. The suspension was mixed with FITC-labelled BSA

and sonicated using a bath sonicator (100W, FS30D, Fisher Scientific) to create OMM vesicles that encapsulate labeled BSA. The vesicles were purified using Amicon Ultra Centrifugal Filter Units (100 kDa molecular weight cutoff, Millipore Sigma). 50 μL of the vesicle suspension was added to the FET surface and allowed to incubate at 37°C for 1 hour. After the incubation period, the excess liquid was removed by pipette aspiration and the FET surface was washed with 1X PBS. The FET was imaged using a fluorescence microscope (Invitrogen, EVOS).

4.10. Detection of Bcl-2 antibodies, ABT-263, and HA14-1 using OMM-FETs

BSA was added onto the OMM-FET to block nonspecific binding sites before adding the test compounds. To detect anti-Bcl-2 antibodies, 10-fold serial dilutions were made from the stock solution using 1X PBS. For each measurement, 1.2 μL of each antibody solution was added to the OMM-FET starting from the lowest concentration and progressing to the highest concentration. Heat denatured (100ºC for 10 min) anti-Bcl-2 antibodies were used as a control.

To detect ABT-263 and HA14-1, 3-fold serial dilutions of the stock solutions were made. ABT-263 solutions at 0.1, 0.3, 0.9, and 2.7 fM were added 1.2 μL at a time onto the FET surface. HA14-1 solutions at 8.1, 24.3, 72.9, and 218.7 fM were added 1.2 μL at a time onto the same device. The current between the drain and the source (I_{ds}) was measured as a function of time. The $\Delta I_{ds}/I_0$ (%) was calculated as $(I_{ds} - I_0)/I_0 \times 100\%$ (I_0 is the initial I_{ds}) and plotted against the drug concentrations.

This thesis is material as it appears in "Nanomaterial biointerfacing via mitochondrial membrane coating for targeted detoxification and molecular detection", Nano Letters 2021, Gong, Hua; Zhang, Qiangzhe; Komarla, Anvita; Wang, Shuyan; Duan, Yaou; Zhou, Zhidong;

Chen, Fang; Fang, Ronnie; Xu, Sheng; Gao, Weiwei; Zhang, Liangfang. The thesis author was a co-author of this paper.

5. References

(1) Zhang, L.; Gu, F. X.; Chan, J. M.; Wang, A. Z.; Langer, R. S.; Farokhzad, O. C. Nanoparticles in Medicine: Therapeutic Applications and Developments. *Clin. Pharmacol. Ther.* **2008**, *83* (5), 761–769. https://doi.org/10.1038/sj.clpt.6100400.

(2) Dehaini, D.; Fang, R. H.; Zhang, L. Biomimetic Strategies for Targeted Nanoparticle Delivery. *Bioeng. Transl. Med.* **2016**, *1* (1), 30–46. https://doi.org/10.1002/btm2.10004.

(3) Sanhai, W. R.; Sakamoto, J. H.; Canady, R.; Ferrari, M. Seven Challenges for Nanomedicine. *Nat. Nanotechnol.* **2008**, *3* (5), 242–244. https://doi.org/10.1038/nnano.2008.114.

(4) Van Haute, D.; Berlin, J. M. Challenges in Realizing Selectivity for Nanoparticle Biodistribution and Clearance: Lessons from Gold Nanoparticles. *Ther. Deliv.* **2017**, *8* (9), 763–774. https://doi.org/10.4155/tde-2017-0057.

(5) Hu, C.-M. J.; Zhang, L.; Aryal, S.; Cheung, C.; Fang, R. H.; Zhang, L. Erythrocyte Membrane-Camouflaged Polymeric Nanoparticles as a Biomimetic Delivery Platform. *Proc. Natl. Acad. Sci. U. S. A.* **2011**, *108* (27), 10980–10985. https://doi.org/10.1073/pnas.1106634108.

(6) Hu, C.-M. J.; Fang, R. H.; Copp, J.; Luk, B. T.; Zhang, L. A Biomimetic Nanosponge That Absorbs Pore-Forming Toxins. *Nat. Nanotechnol.* **2013**, *8* (5), 336–340. https://doi.org/10.1038/nnano.2013.54.

(7) Thamphiwatana, S.; Angsantikul, P.; Escajadillo, T.; Zhang, Q.; Olson, J.; Luk, B. T.; Zhang, S.; Fang, R. H.; Gao, W.; Nizet, V.; Zhang, L. Macrophage-like Nanoparticles Concurrently Absorbing Endotoxins and Proinflammatory Cytokines for Sepsis Management. *Proc. Natl. Acad. Sci.* **2017**, *114* (43), 11488–11493. https://doi.org/10.1073/pnas.1714267114.

(8) Gong, H.; Chen, F.; Huang, Z.; Gu, Y.; Zhang, Q.; Chen, Y.; Zhang, Y.; Zhuang, J.; Cho, Y.-K.; Fang, R. H.; Gao, W.; Xu, S.; Zhang, L. Biomembrane-Modified Field Effect Transistors for Sensitive and Quantitative Detection of Biological Toxins and Pathogens. *ACS Nano* **2019**, *13* (3), 3714–3722. https://doi.org/10.1021/acsnano.9b00911.

(9) Fang, R. H.; Hu, C.-M. J.; Luk, B. T.; Gao, W.; Copp, J. A.; Tai, Y.; O'Connor, D. E.; Zhang, L. Cancer Cell Membrane-Coated Nanoparticles for Anticancer Vaccination and Drug Delivery. *Nano Lett.* **2014**, *14* (4), 2181–2188. https://doi.org/10.1021/nl500618u.

(10) Wang, S.; Duan, Y.; Zhang, Q.; Komarla, A.; Gong, H.; Gao, W.; Zhang, L. Drug Targeting via Platelet Membrane–Coated Nanoparticles. *Small Struct.* **2020**, *1* (1), 2000018. https://doi.org/10.1002/sstr.202000018.

(11) Angsantikul, P.; Thamphiwatana, S.; Zhang, Q.; Spiekermann, K.; Zhuang, J.; Fang, R. H.; Gao, W.; Obonyo, M.; Zhang, L. Coating Nanoparticles with Gastric Epithelial Cell Membrane for Targeted Antibiotic Delivery against Helicobacter Pylori Infection. *Adv. Ther.* **2018**, *1* (2), 1800016. https://doi.org/10.1002/adtp.201800016.

(12) Frezza, C.; Cipolat, S.; Scorrano, L. Organelle Isolation: Functional Mitochondria from Mouse Liver, Muscle and Cultured Filroblasts. *Nat. Protoc.* **2007**, *2* (2), 287–295. https://doi.org/10.1038/nprot.2006.478.

(13) Waite, M. Isolation of Rat Liver Mitochondrial Membrane Fractions and Localization of the Phospholipase A. *Biochemistry* **1969**, *8* (6), 2536–2542. https://doi.org/10.1021/bi00834a041.

(14) Luk, B. T.; Hu, C.-M. J.; Fang, R. H.; Dehaini, D.; Carpenter, C.; Gao, W.; Zhang, L. Interfacial Interactions between Natural RBC Membranes and Synthetic Polymeric Nanoparticles. *Nanoscale* **2014**, *6* (5), 2730–2737. https://doi.org/10.1039/C3NR06371B.

(15) Bhattacharjee, S. DLS and Zeta Potential – What They Are and What They Are Not? *J. Controlled Release* **2016**, *235*, 337–351. https://doi.org/10.1016/j.jconrel.2016.06.017.

(16) Kim, A.; Ng, W. B.; Bernt, W.; Cho, N.-J. Validation of Size Estimation of Nanoparticle Tracking Analysis on Polydisperse Macromolecule Assembly. *Sci. Rep.* **2019**, *9* (1), 2639. https://doi.org/10.1038/s41598-019-38915-x.

(17) Perkins, G.; Renken, C.; Martone, M. E.; Young, S. J.; Ellisman, M.; Frey, T. Electron Tomography of Neuronal Mitochondria: Three-Dimensional Structure and Organization of Cristae and Membrane Contacts. *J. Struct. Biol.* **1997**, *119* (3), 260–272. https://doi.org/10.1006/jsbi.1997.3885.

(18) Mikolajczyk, A.; Gajewicz, A.; Rasulev, B.; Schaeublin, N.; Maurer-Gardner, E.; Hussain, S.; Leszczynski, J.; Puzyn, T. Zeta Potential for Metal Oxide Nanoparticles: A Predictive Model Developed by a Nano-Quantitative Structure–Property Relationship Approach. *Chem. Mater.* **2015**, *27* (7), 2400–2407. https://doi.org/10.1021/cm504406a.

(19) Lindsay, J.; Esposti, M. D.; Gilmore, A. P. Bcl-2 Proteins and Mitochondria—Specificity in Membrane Targeting for Death. *Biochim. Biophys. Acta BBA - Mol. Cell Res.* **2011**, *1813* (4), 532–539. https://doi.org/10.1016/j.bbamcr.2010.10.017.

(20) Mendoza García, M. A.; Izadifar, M.; Chen, X. Evaluation of PBS Treatment and PEI Coating Effects on Surface Morphology and Cellular Response of 3D-Printed Alginate Scaffolds. *J. Funct. Biomater.* **2017**, *8* (4). https://doi.org/10.3390/jfb8040048.

(21) Kavok, N.; Grygorova, G.; Klochkov, V.; Yefimova, S. The Role of Serum Proteins in

the Stabilization of Colloidal LnVO4:Eu3+ (Ln=La, Gd, Y) and CeO2 Nanoparticles. *Colloids Surf. Physicochem. Eng. Asp.* **2017**, *529*, 594–599. https://doi.org/10.1016/j.colsurfa.2017.06.052.

(22) Wendt, M. D. Discovery of ABT-263, a Bcl-Family Protein Inhibitor: Observations on Targeting a Large Protein–Protein Interaction. *Expert Opin. Drug Discov.* **2008**, *3* (9), 1123–1143. https://doi.org/10.1517/17460441.3.9.1123.

(23) Elmore, S. Apoptosis: A Review of Programmed Cell Death. *Toxicol. Pathol.* **2007**, *35* (4), 495–516. https://doi.org/10.1080/01926230701320337.

(24) Tse, C.; Shoemaker, A. R.; Adickes, J.; Anderson, M. G.; Chen, J.; Jin, S.; Johnson, E. F.; Marsh, K. C.; Mitten, M. J.; Nimmer, P.; Roberts, L.; Tahir, S. K.; Xiao, Y.; Yang, X.; Zhang, H.; Fesik, S.; Rosenberg, S. H.; Elmore, S. W. ABT-263: A Potent and Orally Bioavailable Bcl-2 Family Inhibitor. *Cancer Res.* **2008**, *68* (9), 3421–3428. https://doi.org/10.1158/0008-5472.CAN-07-5836.

(25) Tolcher, A. W.; LoRusso, P.; Arzt, J.; Busman, T. A.; Lian, G.; Rudersdorf, N. S.; Vanderwal, C. A.; Waring, J. F.; Yang, J.; Holen, K. D.; Rosen, L. S. Safety, Efficacy, and Pharmacokinetics of Navitoclax (ABT-263) in Combination with Irinotecan: Results of an Open-Label, Phase 1 Study. *Cancer Chemother. Pharmacol.* **2015**, *76* (5), 1041–1049. https://doi.org/10.1007/s00280-015-2882-9.

(26) Birnie, G. D. The HL60 Cell Line: A Model System for Studying Human Myeloid Cell Differentiation. *Br. J. Cancer. Suppl.* **1988**, *9*, 41–45.

(27) Lin, Q.; Que, F.; Gu, C.; Zhong, D.; Zhou, D.; Kong, Y.; Yu, L.; Liu, S. ABT-263 Induces G 1 /G 0 -Phase Arrest, Apoptosis and Autophagy in Human Esophageal Cancer Cells in Vitro. *Acta Pharmacol. Sin.* **2017**, *38* (12), 1632–1641. https://doi.org/10.1038/aps.2017.78.

(28) Schoenwaelder, S. M.; Jarman, K. E.; Gardiner, E. E.; Hua, M.; Qiao, J.; White, M. J.; Josefsson, E. C.; Alwis, I.; Ono, A.; Willcox, A.; Andrews, R. K.; Mason, K. D.; Salem, H. H.; Huang, D. C. S.; Kile, B. T.; Roberts, A. W.; Jackson, S. P. Bcl-XL–Inhibitory BH3 Mimetics Can Induce a Transient Thrombocytopathy That Undermines the Hemostatic Function of Platelets. *Blood* **2011**, *118* (6), 1663–1674. https://doi.org/10.1182/blood-2011-04-347849.

(29) Izak, M.; Bussel, J. B. Management of Thrombocytopenia. *F1000Prime Rep.* **2014**, *6*. https://doi.org/10.12703/P6-45.

(30) Bagamery, K.; Kvell, K.; Landau, R.; Graham, J. Flow Cytometric Analysis of CD41-Labeled Platelets Isolated by the Rapid, One-Step OptiPrep Method from Human Blood. *Cytometry A* **2005**, *65A* (1), 84–87. https://doi.org/10.1002/cyto.a.20133.

(31) Logue, S. E.; Elgendy, M.; Martin, S. J. Expression, Purification and Use of Recombinant Annexin V for the Detection of Apoptotic Cells. *Nat. Protoc.* **2009**, *4* (9), 1383–1395. https://doi.org/10.1038/nprot.2009.143.

(32) Rosi, N. L.; Mirkin, C. A. Nanostructures in Biodiagnostics. *Chem. Rev.* **2005**, *105* (4), 1547–1562. https://doi.org/10.1021/cr030067f.

(33) Liu, S.; Guo, X. Carbon Nanomaterials Field-Effect-Transistor-Based Biosensors. *NPG Asia Mater.* **2012**, *4* (8), e23–e23. https://doi.org/10.1038/am.2012.42.

(34) Gong, H.; Zhang, Q.; Komarla, A.; Wang, S.; Duan, Y.; Zhou, Z.; Chen, F.; Fang, R. H.; Xu, S.; Gao, W.; Zhang, L. Nanomaterial Biointerfacing via Mitochondrial Membrane Coating for Targeted Detoxification and Molecular Detection. *Nano Lett.* **2021**, *21* (6), 2603–2609. https://doi.org/10.1021/acs.nanolett.1c00238.